Circuit Level Modeling of Quasioptical Power Combining Open Cavities

PATRICK L. HERON, GREGORY P. MONAHAN, JEFFREY E. BYRD, MICHAEL B. STEER
Electrical and Computer Engineering Department,
North Carolina State University, Raleigh, NC.

F. W. SCHWERING
United States Army CECOM, Attn. AMSEO-RD-C3-ST, Ft. Monmouth, NJ

J. W. MINK
United States Army Research Office, P.O. Box 12211, Research Triangle Park, NC

ABSTRACT

A multiport circuit level model is developed for an open-cavity, quasioptical power combiner. The model is developed using Hermite-Guassian beam mode theory, the Lorentz reciprocity theorem and determination of diffraction losses.

I. INTRODUCTION

Quasi-optical techniques are attractive means for combining power from numerous solid-state millimeter-wave sources. Power combining is accomplished in free space through superposition of the fields produced by individual radiators which are either globally or locally phase locked. In this paper we present results of a circuit modeling and simulation strategy for quasioptical power combining cavities. Such circuit level modeling and simulation is necessary to obtain a greater insight into the operation of quasioptical power combiners and their somewhat unpredictable locking behavior. The eventual aim is to develop a computer assisted design (CAD) strategy for quasioptical systems. The model is verified through 2 port measurements and field profiling.

In [1] Mink studied an array of filamentary current sources radiating into a plano-concave open resonator. This was the first theoretical investigation of power combining using a source array in a quasi-optical resonator. The results are applicable to the design of resonant cavity quasi-optical combiners and were obtained by use of the Lorentz reciprocity theorem to find the coupling coefficients between the current elements and the natural short-circuit modes of the cavity. The mode coupling coefficients and the radiation resistance were determined for equal and Gaussian weighted sources under the assumption that all modes resonated at a single frequency and that the resonator Q was high. These assumptions are fully removed in this work.

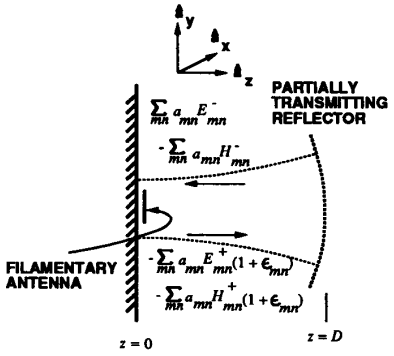

Figure 1: Cross-section of quasioptical resonator.

II. SOURCE ARRAY IMPEDANCE MATRIX

The open cavity power combiner configuration is shown in Fig. 1 and consists of an array of current elements located at $z = d$. The current elements represent small dipoles which are assumed to be driven by active devices. The resonator provides a high Q impedance which allows the individual elements to oscillate at specific frequencies. The oscillating elements are phase locked through the resonator mode structure which accomplishes the power combining. Assuming the paraxial condition holds the fields in the cavity form a complete, ortho-normal system [3]

$$E^{\pm}_{mn}(x,y,z) = \frac{(\mu/\epsilon)^{1/4}}{\sqrt{\pi XY m!n!}}(1+u^2)^{-1/4}(1+v^2)^{-1/4} He_m(\sqrt{2}x/x_s)He_n(\sqrt{2}y/y_s) \exp\left\{-\frac{1}{2}\left[(x/x_s)^2+(y/y_s)^2\right]\right. \mp j\left[kz+\frac{1}{2}\left(u(x/x_s)^2+v(y/y_s)^2\right)\right. \left.\left.-\left(m+\frac{1}{2}\right)\tan^{-1}(u)-\left(n+\frac{1}{2}\right)\tan^{-1}(v)\right]\right\}. \quad (1)$$

K

CH3277-1/93/0000-0433$01.00 © 1993 IEEE

For wave beams propagating in the $\pm\hat{\mathbf{a}}_z$ direction, the H-field is related to the E-field by

$$\mathbf{H}^{\pm}_{mn} = \pm\sqrt{\frac{\epsilon}{\mu}}\hat{\mathbf{a}}_z \times \mathbf{E}^{\pm}_{mn} \tag{2}$$

where,

$$u = \frac{z}{k\bar{X}^2}, \qquad v = \frac{z}{k\bar{Y}^2}$$
$$x_z^2 = \bar{X}^2(1+u^2), \qquad y_z^2 = \bar{Y}^2(1+v^2)$$

the mode parameters are found as[3]

$$\bar{X}^2 = \frac{1}{k}\sqrt{\left(F_x D\left(2-\frac{D}{F_x}\right)\right)}, \quad \bar{Y}^2 = \frac{1}{k}\sqrt{\left(F_y D\left(2-\frac{D}{F_y}\right)\right)}$$

and the following definition of the Hermite polynomials is used:

$$He_n(X) = (-1)^n \exp(X^2/2)\frac{d^n}{dX^n}\left(\exp(-X^2/2)\right). \tag{3}$$

These polynomials form a complete set and satisfy the orthogonality condition

$$\int_{-\infty}^{+\infty} He_s(X)He_m(X)w(X)dX = m!\delta_{sm}\sqrt{2\pi} \tag{4}$$

where the weight function $w(X) = \exp(-X^2/2)$, and δ_{sm} is the Kronecker delta.

An impedance matrix was developed by applying the Lorentz reciprocity theorem to the volume enclosed by two infinite planar surfaces; $\mathbf{S}_1$, the perfectly conducting plane reflector located at $z = 0$, and $\mathbf{S}_2$, an infinite transverse plane located outside the resonator at $z > D$ and using a unit test field incident from $z > D$.

A. Application of Lorentz Reciprocity Theorem

The test field from $z >> D$ (see Fig. 2) is

$$\mathbf{E}_{1,st} = \hat{\mathbf{a}}_x \begin{cases} c_{st}(E^-_{st} - E^+_{st}) & ; \ 0 < z < D \\ (E^-_{st} + b_{st}E^+_{st}) & ; \ z > D \end{cases}, \tag{5}$$

and using the transmission and reflection coefficients at the reflector surfaces yields

$$c_{st}E^-_{st} = T_{st}E^-_{st} - c_{st}R_{st}E^+_{st}$$

and,

$$b_{st}E^+_{st} = R_{st}E^-_{st} - c_{st}T_{st}E^+_{st}.$$

Solving for c_{st} and b_{st}

$$c_{st} = \frac{T_{st}}{1 + R_{st}\psi_{st}} \tag{6}$$

and,

$$b_{st} = \frac{R_{st}}{\psi_{st}} - \frac{T^2_{st}}{1 + R_{st}\psi_{st}}. \tag{7}$$

where $\psi_{st} \equiv E^+_{D,st}/E^-_{D,st}$, and the notation $E^{\pm}_{D,st}$ is used to indicate $E^{\pm}_{st}$ evaluated on the surface of the spherical reflector.

The fields, $\mathbf{E}_2$ and $\mathbf{H}_2$ are excited by an array of $\hat{\mathbf{a}}_x$ directed current sources $\mathbf{J}_2$ as shown in Fig. 1 and consist of a standing wave and a travelling wave components:

$$\mathbf{E}_2 = \hat{\mathbf{a}}_x \sum_{mn} \begin{cases} f_{mn}(E^-_{mn} - E^+_{mn}) & ; \ 0 \le z < d \\ a_{mn}(E^-_{mn} - (1+\varepsilon_{mn})E^+_{mn}) & ; \ d < z \le D \\ g_{mn}E^+_{mn} & ; \ z > D \end{cases}. \tag{8}$$

The reflector characteristics are again applied along with (8) to find

$$\varepsilon_{mn} = -\frac{1}{\psi_{mn}R_{mn}} - 1 \tag{9}$$

and

$$a_{mn} = \frac{g_{mn}\psi_{mn}R_{mn}}{T_{mn}}. \tag{10}$$

Now equating the modal fields at $z = d$ we get

$$f_{mn} = a_{mn}\frac{(1 + \Upsilon_{mn}/(R_{mn}\psi_{mn}))}{(1 - \Upsilon_{mn})}. \tag{11}$$

Where the ratio $\Upsilon_{mn} \equiv E^+_{mn}/E^-_{mn}$ is evaluated at $\{x, y, z\} = \{0, 0, d\}$. Near the surface $z = 0$ the phase fronts of E^+_{mn} and E^-_{mn} are nearly planar so for fixed z, Υ_{mn} is approximately independent of x and y.

The reciprocity theorem is now applied over the volume bounded by $\mathbf{S} = \mathbf{S}_1 + \mathbf{S}_2$ to find the relationship between $\mathbf{J}_2$ and g_{mn} and so

$$2g_{mn} = \frac{-T_{mn}}{1 + R_{mn}\psi_{mn}}\int_V (E^-_{mn} - E^+_{mn})\hat{\mathbf{a}}_x \cdot \mathbf{J}_2 dV. \tag{12}$$

This result relates the modal source fields to the current of the array elements. The expression (12) assumes that $\mathbf{E} = \hat{\mathbf{a}}_x E$ and thus $\mathbf{J}_2 = \hat{\mathbf{a}}_x J_2$. For a general $\mathbf{J}_2$ confined to a transverse plane, an $\hat{\mathbf{a}}_y$ polarization term for E must be included in (8) and (5). The reciprocity calculation then proceeds as before.

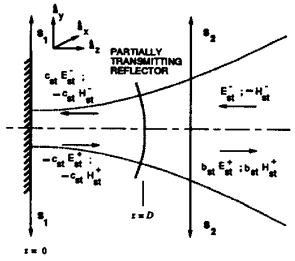

Figure 2: Cross-Section of Quasioptical Resonator Showing Fields, $\mathbf{E}_2$, Established by Radiating Current Elements.

B. Diffraction and Conductor Losses

The diffraction losses are included in the model by incorporating them into the reflection coefficient, R_{mn}, of the spherical reflector. The power loss per transit due to diffraction, α_{mn}, is [2]

$$\alpha_{mn} = 1 - |\chi_m\chi_n|^2 = 1 - \left|\frac{2c}{\pi}R^{(1)}_{0,m}(c,1)R^{(1)}_{0,n}(c,1)\right|^2. \tag{13}$$

Where $R_{0n}^{(1)}$ is the prolate spheroidal radial wave function, and $c = a^2k/b$ for reflectors having radius of curvature b and an aperture of dimension $2a$. The fields are evaluated at discrete points on the reflectors and Simpson's rule is used to perform the integration. This is the same method used by Soohoo [4] except that it has been extended to include rectangular apertures, and also allows for different x and y focal lengths. Thus an effective reflection coefficient

$$\Gamma_{mn} = |\chi_m \chi_n| R_{mn} \tag{14}$$

is computed. In a simulation environment the speed of the diffraction loss calculation is increased by modeling the resonator mode electric field transition gain, $|\chi_m \chi_n|$, using

$$|\chi_m \chi_n| = \sqrt{(1 - A_m 10^{-B_m c_x})(1 - A_n 10^{-B_n c_y})} \tag{15}$$

where the constants A_n, A_m, B_m, B_n are determined numerically, and $c_{x,y} = ka_{x,y}^2/2D$, and a is the aperture half-width. Conductor losses were determined by the usual surface resistance calculation. and included in Γ_{mn}.

C. Impedance Matrix

The multi-port model is described by its z parameters such that

$$\mathbf{V} = \mathbf{ZI} \tag{16}$$

It is desirable to model the resonator and antenna array as a linear multiport circuit for purposes of computer-aided quasi-optical power combiner analysis and design. Each port of the cuit corresponds to the terminals of a particular antenna with the p *th* antenna located at $\{x, y, z\} = \{x_p, y_p, z_p\}$. For this array, (12) takes the very simple form

$$2g_{mn} = \frac{-T_{mn}}{(1 + R_{mn}\psi_{mn})} \sum_q I_q \Delta X_q (E_{q,mn}^- - E_{q,mn}^+). \tag{17}$$

Where $E_{q,mn}^{\pm}$ is $E_{mn}^{\pm}$ evaluated at $\{x_q, y_q, z_q\}$, and I_q and ΔX_q are the terminal current and effective length of the q*th* dipole respectively.

The driving point impedance of the p*th* dipole in the presence of all other dipoles is found by use of a reaction principle [6]

$$Z_p = -\frac{1}{I_p^2} \int_V \mathbf{J}_p \cdot \mathbf{E}_2 dV. \tag{18}$$

$$z_{pq} = \frac{\Delta X_p \Delta X_q}{2} \sum_{mn} \left[\frac{(R_{mn}\psi_{mn} + \Upsilon_{mn})}{(1 + R_{mn}\psi_{mn})(1 - \Upsilon_{mn})} (E_{p,mn}^- - E_{p,mn}^+)(E_{q,mn}^- - E_{q,mn}^+) \right]. \tag{19}$$

This impedance is the contribution of the paraxial fields. Nonparaxial fields are not important for determining the self-impedance of a radiating element but are important in describing antenna-to-antenna coupling. This effect is incorporated by considering half-space ratiaion in the next section.

D. Nonresonant Field Contribution

The cavity resonant impedance as derived in the previous section describes the coupling between an electric current density and the cavity modal fields. In the derivation of the traveling wavebeams, far field radiation was assumed as well as paraxial propagation. In the absence of the curved reflector, these fields would comprise radiating fields which diverge from the z axis by a small angle. In general, a current distribution located over a ground plane will produce some nonparaxial radiation as well as some near field components which have intensity that decreases faster than $1/r$. The impedance contributions of these nonresonant fields must be added to the impedance due to the resonant fields to determine the total impedance.

The impedance contribution of the nonresonant fields is derived by assuming that the non-resonant field structure near the plane $z = d$ and close to the z axis is essentially unchanged if the spherical reflector is removed. This assumption is justifiable because much of the radiating nonparaxial energy falls outside the spherical reflector aperture, also most of the nonparaxial energy that impinges on the spherical reflector diverges from the z axis after reflection and does not return to the region of the source current. Also, the amount of energy reflected back to the source due to the near field terms is negligible because the reflectors are assumed to be in each other's far field.

If the spherical reflector is removed a half-space remains, bounded by the perfectly conducting planar reflector. The field components that comprised the cavity modal fields become, in the half space, radiating paraxial wavebeams.

In order not to account for the paraxial fields twice the impedance contribution of the quasioptic fields with $R_{m,n} = 0$ must be subtracted from (19) resulting in

$$z'_{pq} = \frac{\Delta X_p \Delta X_q}{2} \sum_{mn} \left[\frac{R_{mn}\psi_{mn}}{(1 + R_{mn}\psi_{mn})} (E_{p,mn}^- - E_{p,mn}^+)(E_{q,mn}^- - E_{q,mn}^+) \right]. \tag{20}$$

Thus the circuit equation (16) becomes

$$\mathbf{V} = \mathbf{ZI} = \left(\mathbf{Z}_{\text{RESONANT}} + \mathbf{Z}_{\text{NON-RESONANT}}\right) \mathbf{I} \tag{21}$$

where the elements of $\mathbf{Z}_{\text{RESONANT}}$ are z'_{pq} and the elements of $\mathbf{Z}_{\text{NON-RESONANT}}$ for now must be evaluated numerically using the dyadic half-space Green's function which represents all the field components generated by an electric source current density; traveling paraxial wavebeams , nonparaxial fields, and nonradiating fields.

III. Computed Results And Experiment

Measurements were made using an electrically short inverted L antenna. The first step in verifying the impedance matrix presented above is to identify the cavity modes. Figs. 3 and 4 are field profiels of two modes at their resonant frequencies. These profiles indicate that Gauss-Hermite modes are established and are highly regular. The slight asymmetry is attributed to the offset of the exciting antenna. For each longitudinal mode index, q, the transverse electromagnetic modes; TEM_{00}, TEM_{10}, TEM_{01}, TEM_{20}, TEM_{02}, and

TEM_{11} were observed. The response for higher transverse mode numbers was very small due to diffraction losses. One-port and two-port measurements were made for each of these modes for the $q = 35$ family and compare very well with simulated results as seen in Fig. 5. The importance of including the non-paraxial fields is seen in Fig. 6.

REFERENCES

[1] J. W. Mink, "Quasi-Optical Power Combining of Solid-State Millimeter-Wave Sources," *IEEE Trans on Microwave Theory and Tech.*, vol MTT-34 Feb, 1986, pp. 273-279.

[2] G. D. Boyd and J. P. Gordon, "Confocal Multimode Resonator Theory for Millimeter Through Optical Wavelength Masers," *Bell Sys. Tech. Jour.*, March 1961, pp.489-509.

[3] G. Goubau, "Beam Waveguides," in *Advances in Microwaves*,vol.3, New York: Academic Press 1968, pp 67-126.

[4] R. F. Soohoo,"Nonconfocal Multimode Resonators for Masers," *Proceedings of IEEE*, Jan.1963, pp.70-75.

[5] A.R. Djordjevic, T.K. Sarkar and Roger F. Harrington, "Time-domain response of multiconductor transmission lines," Proc. I.E.E.E., **75**, pp. 743-764, June 1987.

[6] C. A. Balanis, *Antenna Theory, Analysis and Design*, Harper and Row, 1982.

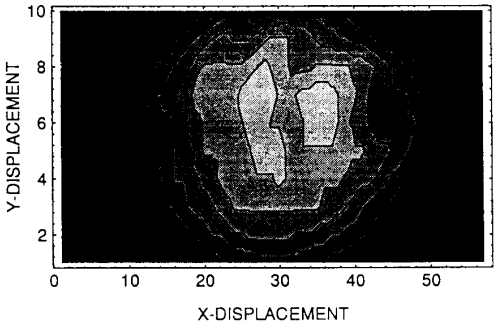

Figure 3: Measured Relative Field Strength for the $TEM_{0,0,35}$ Mode.

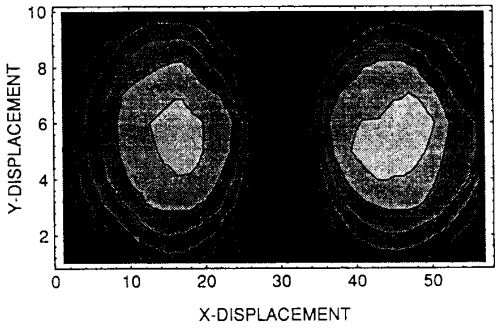

Figure 4: Measured Relative Field Strength for the $TEM_{1,0,35}$ Mode.

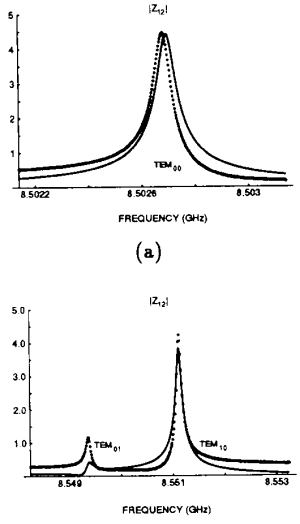

Figure 5: Measured and Simulated Values of $|z_{12}|$ for: (a) modes TEM_{02}, TEM_{11}, TEM_{20}; and (b) modes TEM_{01}, TEM_{10}.

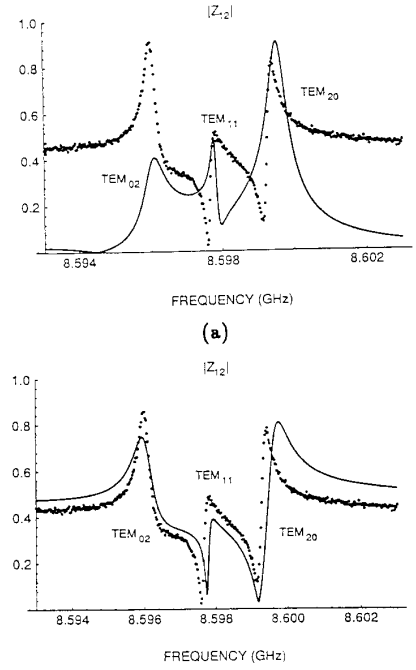

Figure 6: Measured and Simulated Values of $|z_{12}|$: (a) without considering non-paraxial modes; and (b) considering non-paraxial modes.